

1 **On the barium - oxygen consumption relationship in the Mediterranean Sea: implications**
2 **for mesopelagic marine snow remineralisation.**

3
4 Stéphanie H.M. Jacquet^{1*}, Dominique Lefèvre¹, Christian Tamburini¹, Marc Garel¹, Frédéric
5 A.C. Le Moigne¹, Nagib Bhairy¹, Sophie Guasco¹

6
7 ¹Aix Marseille Université, CNRS/INSU, Université de Toulon, IRD, Mediterranean Institute of
8 Oceanography (MIO), UM 110, 13288 Marseille, France,

9
10 *Correspondence to: S. Jacquet (*stephanie.jacquet@mio.osupytheas.fr*)

11
12
13 Biogeosciences

14
15
16
17

18 **ABSTRACT**

19 In the ocean, remineralisation rate associated with sinking particles is a crucial variable. Since
20 the 90's, particulate biogenic barium (Ba_{xs}) has been used as an indicator of carbon
21 remineralization by applying a transfer function relating Ba_{xs} to O_2 consumption (Dehairs's
22 transfer function, Southern Ocean-based). Here, we tested its validity in the Mediterranean Sea
23 (ANTARES / EMSO-LO) for the first time by investigating connections between Ba_{xs} ,
24 prokaryotic heterotrophic production (PHP) and oxygen consumption (JO_2 -Opt; optodes
25 measurement). We show that: (1) higher Ba_{xs} (409 pM; 100- 500 m) occurs in situations where
26 integrated PHP ($PHP_{100/500} = 0.90$) is located deeper, (2) higher Ba_{xs} occurs with increasing
27 JO_2 -Opt, and (3) similar magnitude between JO_2 -Opt ($3.14 \text{ mmol m}^{-2} \text{ d}^{-1}$; 175- 450 m) and JO_2 -
28 Ba ($4.59 \text{ mmol m}^{-2} \text{ d}^{-1}$; transfer function). Overall, Ba_{xs} , PHP and JO_2 relationships follow trends
29 observed earlier in the Southern Ocean. We conclude that such transfer function could apply in
30 the Mediterranean Sea.

31

32

33 **KEY WORDS:** particulate biogenic barium, mesopelagic zone, oxygen consumption,
34 prokaryotic heterotrophic production, carbon remineralization, Mediterranean Sea

35

36 **1. INTRODUCTION**

37 Ocean ecosystems play a critical role in the Earth's carbon (C) cycle [IPCC, 2014]. The
38 quantification of their impacts of both present conditions and future predictions remains one of
39 the greatest challenges in oceanography [Siegel et al., 2016]. In essence, the biological C pump is
40 termed for the numerous processes involved in maintaining the vertical gradient in dissolved
41 inorganic C. This includes processes such as organic matter production in surface, its export and
42 subsequent remineralization. Most of marine snow organic C conversion (i.e. remineralization)
43 into CO₂ by heterotrophic organisms (i.e. respiration) occurs in the mesopelagic zone (100-1000
44 m) [Martin et al., 1987; Buesseler and Boyd, 2009]. Globally, the flux of C exported below 1000
45 m depth is the key determinant of ocean carbon storage capacity [Henson et al., 2011]. However,
46 there is no consensus on C transfer efficiency estimations from field experiments, leading to an
47 imbalance of the water column C budget [Giering et al., 2014]. Resolving this imbalance is in the
48 core of numerous studies in the global ocean, but also regionally, especially in the Mediterranean
49 Sea (MedSea). Due to limited exchanges with adjacent basin and the existence of an intense
50 overturning circulation qualitatively resembling the global one (but with shorter time scales), the
51 MedSea is often considered as a laboratory to observe and understand the impact of transient
52 climate variability on ecosystems and biogeochemical cycles [Malanotte-Rissoli et al., 2014]. In a
53 context of climate changes, better constraining C fluxes and the ocean C storage capacity is of
54 crucial importance.

55 Particulate barium in excess (Ba_{xs}, i.e. biogenic Ba from total particulate Ba after correction for
56 lithogenic Ba) is a geochemical tracer of particulate organic carbon (POC) remineralization in the
57 mesopelagic layer [Dehairs et al., 1997]. Ba_{xs} mostly occurs in the form of barite microcrystals
58 (BaSO₄) at these depths. In a global ocean undersaturated with respect to barite, studies report
59 that Ba_{xs} would precipitate inside oversaturated biogenic micro-environments during POC

60 degradation by heterotrophic prokaryotes in the mesopelagic zone, through sulfate and/or barium
61 enrichment [Bertram and Cowen, 1997]. The first-ever studies on mesopelagic Ba_{xs} reported
62 coinciding Ba_{xs} maxima with depths of dissolved O_2 minimum and pCO_2 maximum [Dehairs et
63 al., 1987, 1997]. By using an 1D advection-diffusion model applied to O_2 profiles in the Atlantic
64 sector of the Southern Ocean (ANTX/6 cruise; Shopova et al., 1995), Dehairs et al. [1997]
65 established an algorithm converting mesopelagic Ba_{xs} concentration into O_2 consumption rate
66 (JO_2) and organic C remineralized (POC remineralization rate). This transfer function has been
67 widely used until now [Cardinal et al., 2001, 2005; Dehairs et al., 2008; Jacquet et al., 2008a,
68 2008b, 2011, 2015]. Yet its validity has never been tested in other oceanic provinces. In the
69 North Atlantic, Lemaitre et al. [2018] reported a Ba_{xs} - JO_2 (obtained from apparent oxygen
70 utilisation divided by the water mass age) relationship not significantly different to that reported
71 in Dehairs et al. [1997]. Furthermore, significant progresses were made in relating Ba_{xs} , O_2
72 dynamics to prokaryotic heterotrophic activity [Jacquet et al., 2015]. These advancements clearly
73 show that Ba_{xs} is closely related with the vertical distribution of prokaryotes heterotrophic
74 production (PHP) (the rate of change with depth), reflecting the temporal progression of POC
75 remineralization processes. Also, in a first attempt to test the validity of the Dehairs's transfer
76 function in other locations, Jacquet et al. [2015] confronted oxygen consumption rates (JO_2) from
77 direct measurements (dark community respiration, DCR) to derived JO_2 from Ba_{xs} data (using the
78 transfer function) in the Kerguelen area (Indian sector of the Southern Ocean). We revealed good
79 convergence of JO_2 rates from these two approaches, further supporting the Dehairs's function to
80 estimate POC remineralization rates in different biogeochemical settings of the Southern Ocean.

81 Here, we further investigate relationships between the mesopelagic Ba_{xs} proxy, prokaryotic
82 activity and oxygen dynamics (Figure 1a) in the northwestern Mediterreanean Sea (MedSea), a
83 different biogeochemical setting to those already studied (see references above). Today,

84 observations of the various components of the MedSea biological C pump provide organic C
85 remineralization fluxes varying by at least an order of magnitude [Santinelli et al., 2010;
86 Ramondenc et al., 2016]. Malanotte-Rissoli et al. [2014] reviewing unsolved issues and future
87 directions for MedSea research highlighted the need to further investigate biogeochemical
88 processes at intermediate (mesopelagic) and deep layers to reconcile the C budget in the
89 Mediterranean basin. Previous particulate Ba_{xs} dataset is very scarce in the NW- MedSea, with in
90 general very low vertical sampling resolution [Sanchez Vidal et al., 2005] or very restricted
91 studied areas [Dehairs et al., 1987; Sternberg et al., 2008]. Here we discuss Ba_{xs} , PHP and JO_2
92 (from optodes measurement during incubations) at the ANTARES / EMSO-LO observatory site
93 (Figure 1a, b). We hypothesize that the Dehairs's transfer function converting Ba_{xs} into POC
94 remineralization also applies in a different ocean ecosystem functioning from the Southern
95 Ocean. We suggest that the Ba_{xs} proxy can be used as routine tracer to estimate local-scale
96 processes of mesopelagic POC remineralization in the Mediterranean basin.

97

98 **2. METHODS**

99 **2.1 STUDY SITE**

100 The BATMAN cruise (<https://doi.org/10.17600/16011100>, March 10-16 2016, *R/V EUROPE*)
101 took place to the ANTARES / EMSO-LO observatory site (42°48'N, 6°10'E; Tamburini et al.,
102 2013), 40 km off the coast of Toulon, southern France (Figure 1b). The hydrological and
103 biogeochemical conditions at this site are monitored monthly in the framework of the MOOSE
104 (Mediterranean Ocean Observing System for the Environment) program and of the EMSO
105 (European Multidisciplinary Subsea Observatory) observation program. The hydrography
106 displays the general three-layer MedSea system with surface, intermediate and deep waters
107 [Hainbucher et al., 2014]. Briefly, the main water masses can be distinguished (see potential

108 temperature – salinity diagram during the BATMAN cruise in Figure 1c): (1) Surface Water
109 (SW); (2) Winter Intermediate Water (WIW); (3) Levantine Intermediate water (LIW). LIW is
110 present at intermediate depths (around 400 m at ANTARES) and is characterized by temperature
111 and a salinity maxima; (4) Mediterranean Deep Water (MDW).

112

113 **2.2 SAMPLING AND ANALYSES**

114 For particulate barium, 4 to 7 L of seawater sampled using Niskin bottles were filtered onto 47
115 mm polycarbonate membranes (0.4 μm porosity) under slight overpressure supplied by filtered
116 air. Filters were rinsed with few mL of Milli-Q grade water to remove sea salt, dried (50°C) and
117 stored in Petri dishes. Thirteen depths between surface and 1000 m were sampled by combining
118 different casts sampled closely in time and space (total of 28 samples) with similar potential
119 temperature – salinity profiles. No major changes in water mass characteristics occurred over the
120 3-day sampling period (Figure 1c). In the laboratory, we performed a total digestion of filters
121 using a concentrated tri-acid (0.5 mL HF /1.5 mL HNO₃ / HCl 1 mL; all Optima grade) mixture
122 in closed teflon beakers overnight at 95°C in a clean pressurized room. After evaporation close to
123 dryness, samples were re-dissolved into 10 mL of HNO₃ 2%. The solutions were analysed for Ba
124 and other elements of interest (Na and Al) by HR-ICP-MS (High Resolution-Inductively Coupled
125 Plasma- Mass Spectrometry; ELEMENT XR ThermoFisher). Based on analyses of external
126 certified reference standards, accuracy and reproducibility were both within $\pm 5\%$. Details on
127 sample processing and analysis are given in Cardinal et al. [2001] and Jacquet et al. [2015]. The
128 presence of sea-salt was checked by analysing Na and the sea-salt particulate Ba contribution was
129 found negligible (<0.1% of total Ba). Particulate biogenic barium in excess (hereafter referred to
130 as Ba_{xs}) was calculated as the difference between total Ba and lithogenic Ba using Al as the
131 lithogenic reference element. The lithogenic Ba concentration was determined using Al

132 concentration and the upper continental crust (UCC) Ba:Al molar ratio [Taylor and Mc.Lennan,
133 1985]. The biogenic Ba fraction ranged from 51 to 91 % of the total particulate Ba signal (see
134 section 3.1). The standard uncertainty [Ellison et al., 2000] on Ba_{xs} concentration ranges between
135 5.0 and 5.5%. The term “in excess” is used to indicate that concentrations are larger than the Ba_{xs}
136 background. The background (or residual value) is considered as “preformed” Ba_{xs} at zero
137 oxygen consumption left over after transfer and partial dissolution of Ba_{xs} produced during
138 degradation of previous phytoplankton growth events. The background is set at 130 pM in this
139 study.

140 Oxygen concentrations were measured using oxygen optode Aanderaa® 4330 for at least 24
141 hours (on a 30 seconds time step) on samples taken at 4 depths in the mesopelagic layer (175,
142 250, 450 and 1000 m). Samples were placed into a sealed 1L borosilicate glass bottles incubated
143 at a constant temperature of 13°C in thermo-regulated baths. Optodes were calibrated using a
144 home made calibration facility (<https://www.mio.osupytheas.fr/en/cybele/oxygen-dynamics-construction-oxygen-optode-calibration-platform>). Oxygen consumption rates (later referred to as
145 $\text{JO}_2\text{-Opt}$) were derived from a linear model calculation. Associated errors to the linear model fit
146 are below 0.01 $\mu\text{M O}_2 \text{ h}^{-1}$. Each oxygen consumption experiment has been duplicated for each
147 depth. Average and standard deviation of the duplicates are reported in Fig 3a. The larger
148 associated errors are related to the differences between each duplicates, especially in surface,
149 reflecting potential heterogeneity of the microbial community during sampling.

151 Prokaryotic heterotrophic production (PHP) estimation was measured over time course
152 experiments at in situ temperature (13°C) following the protocol described in Tamburini et al.
153 [2002]. 3H-leucine labelled tracer [Kirchman, 1993] was used. For water sample collected with
154 Niskin bottle we have performed measurement in three replicate 20 mL and 40 mL seawater
155 volume for the depth ranged 0 to 800 m-depth with 20nM at final concentration of Leucine.

156 Concerning depth above 800 m-depth, PHP was measured in three replicate of 40 mL of seawater
157 with 10nM at final concentration of Leucine. Samples were incubated 2, 6 and 10 hours
158 respectively for sample ranged between 0-200 m, 200-600 m and up 800 m-depth. To calculate
159 prokaryotic heterotrophic production, we used the empirical conversion factor of 1.55 ng C per
160 pmol of incorporated leucine according to Simon and Azam [1989], assuming that isotope
161 dilution was negligible under these saturating concentrations.

162

163 **3. RESULTS AND DISCUSSION**

164 **3.1 Particulate Ba_{xs} vertical distribution**

165 Particulate biogenic Ba_{xs}, particulate Al (pAl) and biogenic Ba fraction profiles in the upper
166 1000 m at ANTARES are reported in Figure 2a. Ba_{xs} concentrations range from 12 to 719 pM.
167 The biogenic Ba fraction ranges from 51 to 91 % of the total particulate Ba signal. Particulate Al
168 concentrations (pAl) range from 8 to 170 nM. Ba_{xs} concentrations are low in surface water (<100
169 pM) where the lithogenic fraction reaches 43 to 49 % in the upper 70 m. From previous studies
170 we know that Ba_{xs} in surface waters is distributed over different, mainly non-barite biogenic
171 phases, and incorporated into or adsorbed onto phytoplankton material. As such these do not
172 reflect POC remineralization processes, in contrast to mesopelagic waters where Ba_{xs} is mainly
173 composed of barite formed during prokaryotic degradation of organic matter. Focus is done in the
174 present study on the mesopelagic layer. The Ba_{xs} profile at ANTARES indeed displays a
175 mesopelagic Ba_{xs} maximum between 100 and 500 m, reaching up to 719 pM at 175 m. Ba is
176 mostly biogenic at these depths (> 80 %). Ba_{xs} concentrations then decrease below 500 m to
177 reach a background value of around 130 pM (see BKG in Figure 2). Note that the MedSea is
178 largely undersaturated with respect to barite, with saturation state ranging between 0.2 and 0.6
179 over the basin [Jacquet et al., 2016; Jullion et al., 2017]. For comparison, the Ba_{xs} background

180 value in the Southern Ocean reaches 180 to 200 pM below 1000 m [Dehairs et al., 1997; Jacquet
181 et al. 2015]. Previously, Sternberg et al. [2008] reported the seasonal evolution of Ba_{xs} profiles at
182 the DYFAMED station (43°25'N-7°52'E; BARMED project) northeast from ANTARES (Figure
183 1c) in the NW-MedSea. The present Ba_{xs} profile at ANTARES (March 2016) is very similar to
184 the Ba_{xs} profile measured in March 2003 at DYFAMED (Figure 2a). The slight difference
185 between Ba_{xs} profiles in the upper 75 m suggests more Ba bounded and/or adsorbed onto
186 phytoplankton material during BARMED. Both profiles present a Ba_{xs} maximum in the upper
187 mesopelagic zone between 150 and 200 m. Below this maximum, Ba_{xs} concentrations gradually
188 decrease to reach around 130 pM between 500 and 1000 m (this study). A similar value was
189 reached between 500 and 600 m at the DYFAMED station over the whole studied period
190 (between February and June 2003; Sternberg et al., 2008).

191

192 **3.2 Prokaryotic heterotrophic production**

193 The particulate Ba in excess is centred in the upper mesopelagic zone between 100 and 500 m
194 and reflects that POC remineralization mainly occurred at this depth layer (Figure 2a). Depth-
195 weighted average (DWA) Ba_{xs} content (409 pM), i.e. the Ba_{xs} inventory divided by the depth
196 layer considered, was calculated between 100 and 500 m. Figure 2b shows the column-integrated
197 PHP at 100 m over the one at 500 m (PHP100/500). Our PHP100/500 ratio at ANTARES station
198 is of 0.90 and is compared to results obtained during KEOPS1 (summer) and KEOPS2 (spring;
199 out plateau stations) cruises in the Southern Ocean [Jacquet et al., 2008; 2015] and #DY032
200 cruise (July 2015, *R/V DISCOVERY*) at the PAP (Porcupine Abyssal Plain) observatory in the
201 northeast Atlantic (49°N, 16.5 °W) (personal data). Result at the ANTARES / EMSO-LO site
202 follows the trend previously reported in the Southern Ocean (blue line in Figure 2b; Jacquet et al.,
203 2015), indicating higher DWA Ba_{xs} in situations where a significant part of column-integrated

204 PHP is located deeper in the water column (high Int. PHPx1/IntPHPx2 ratio; Figure 2b). These
205 previous studies revealed that the shape of the column-integrated PHP profile (i.e. the attenuation
206 gradient) is important in setting the Ba_{xs} signal in the mesopelagic zone (Dehairs et al., 2008;
207 Jacquet et al., 2008, 2015]. Indeed, mesopelagic DWA Ba_{xs} appears reduced when most of the
208 column-integrated PHP is limited to the upper layer, i.e. indicating an efficient remineralization
209 in surface. In contrast, mesopelagic DWA Ba_{xs} appears higher when most of the column-
210 integrated PHP is located in the mesopelagic layer, i.e. reflecting significant deep PHP activity,
211 POC export and subsequent remineralization (Figure 2b). Results at the PAP site reflect a similar
212 situation as observed during KEOPS2 for time series stations at Plateau site and in a meander of
213 the polar front area (not show in Figure 2b). At these stations, Jacquet et al. [2015] reported a
214 shift toward the KEOPS1 trend reflecting the temporal evolution (season advancement) and
215 patchiness of the establishment of mesopelagic remineralization processes within a same area.
216 Overall, our MedSea result is located along the trend defined in the Southern Ocean during
217 KEOPS1 cruise. It is generally considered that Ba_{xs} (barite) forms inside sulfate and/or barium
218 oversaturated biogenic micro-environments during POC degradation by heterotrophic
219 prokaryotes. However, it is unclear whether barite formation at mesopelagic depths is (directly or
220 indirectly) bacterially induced or bacterially influenced [Martinez-Ruiz et al., 2018, 2019]. In any
221 case our results strengthen the close link between the water column Ba_{xs} distribution and
222 respiration (organic matter degradation).

223

224 **3.3 Oxygen- barium relationship**

225 The relationship we obtained at ANTARES between Ba_{xs} concentrations and oxygen
226 consumption rates from optodes measurements ($\text{JO}_2\text{-Opt}$) is reported in Figure 3a. $\text{JO}_2\text{-Opt}$ range
227 from 0.11 to 5.85 $\mu\text{mol L}^{-1} \text{ d}^{-1}$. The relationship indicates higher Ba_{xs} concentrations with

228 increasing JO_2 -Opt. An interesting feature is the intercept at zero JO_2 -Opt (around 128 pM)
229 which further supports the Ba BKG value at ANTARES (130 pM) determined from measured
230 Ba_{xs} profiles (Figure 3a).

231 In figure 3b we applied a similar approach as reported in Jacquet et al. [2015] where we show
232 the correlation between JO_2 obtained from dark community respiration DCR (Winkler titration;
233 JO_2 -DCR) data integration in the water column and JO_2 based on Ba_{xs} content (Dehairs's transfer
234 function; later referred to as JO_2 -Ba). Similarly, to estimate JO_2 -Ba in the present study we used
235 the following equation [Dehairs et al., 1997] (Figure 3c):

236
$$\text{JO}_2\text{-Ba} = (\text{Ba}_{\text{xs}} - \text{Ba BKG})/17450 \quad (1)$$

237 A Ba BKG value of 130 pM was used (see above). JO_2 -Ba is confronted to JO_2 -Opt integrated
238 over the same layer depth (between 175 and 450 m; Figure 3b). JO_2 rates are of the same order of
239 magnitude ($\text{JO}_2\text{-Ba} = 4.59 \text{ mmol m}^{-2} \text{ d}^{-1}$ and $\text{JO}_2\text{-opt} = 3.14 \text{ mmol m}^{-2} \text{ d}^{-1}$). The slight difference
240 could be explained by the integration time of both methods: few hours to days for the incubations
241 vs. few days to weeks for Ba_{xs} (seasonal build-up; Jacquet et al., 2007). JO_2 rates calculated in the
242 present work are 3 times higher than those reported in the Southern Ocean during KEOPS1
243 [Jacquet et al., 2015] but they are in good agreement with the Ba_{xs} vs JO_2 trend (Figure 3b).
244 DWA Ba_{xs} and JO_2 measured during KEOPS1 [Jacquet et al., 2015] and at ANTARES site (this
245 study) are compared to Dehairs's relationship in Figure 3c. The correlation obtained in Lemaitre
246 et al. [2018] in the North Atlantic is also reported (JO_2 were calculated from apparent oxygen
247 utilisation divided by water mass age). Note that this relationship is not significantly different
248 from the Dehairs's equation [Lemaitre et al., 2018]. Overall, results at the ANTARES site are
249 lying along the Southern Ocean Ba_{xs} - JO_2 correlation. This further supports the validity of the
250 Dehairs's transfer function in the present study.

251

252 **3.4 Estimated particles remineralisation rates and implications**

253 In order to provide a Ba_{xs} -derived estimate of POC remineralization rate (MR) at the
254 ANTARES / EMSO-LO observatory during BATMAN cruise, we converted $\text{JO}_2\text{-Ba}$ into C
255 respired using the Redfield (RR) C/O₂ molar ratio (127/175; Broecker et al., 1985) multiplied by
256 the depth layer considered (Z, 175-450 m) [Dehairs et al., 1997]:

257
$$\text{MR} = Z \times \text{JO}_2\text{-Ba} \times \text{RR} \quad (2)$$

258 We obtain a POC remineralization rate of 11 mmol C m⁻² d⁻¹ (10% RSD). This is within the
259 range of dissolved Ba- derived fluxes of POC remineralization (13 to 29 mmol C m⁻² d⁻¹)
260 reported in the Mediterranean Sea previously [Jacquet et al., 2016; Jullion et al., 2017].
261 Following calculations reported in Jullion et al. [2007], our MR rate would correspond to a Ba_{xs}
262 flux of around 0.01 $\mu\text{mol m}^{-2} \text{d}^{-1}$. This is in reasonable agreement with barium fluxes (0.01 to
263 0.08 $\mu\text{mol m}^{-2} \text{d}^{-1}$) presented in Jullion et al. [2007]. Previously published barium fluxes from
264 sediment trap range from 0.27 to 0.36 $\mu\text{mol m}^{-2} \text{d}^{-1}$ at the DYFAMED station [Sternberg et al.,
265 2007] and from 0.39 to 1.07 $\mu\text{mol m}^{-2} \text{d}^{-1}$ in the Alboran Sea [Sanchez-Vidal et al., 2005]. POC
266 remineralization rate from the present study is in the range of previously published carbon export
267 fluxes (few to tens mmol m⁻² d⁻¹) from thorium-derived data [Speicher et al., 2006] or from
268 combining drifting sediment traps and underwater vision profilers [Ramondenc et al., 2016].
269 Constraining POC flux attenuation and remineralization rates in the Mediterranean is far from
270 being achieved, especially regarding seasonal changes and inter-basin variations, but the
271 concordance of the different approaches is promising.

272

273 **4. CONCLUSIONS**

274 The present paper brings a first insight into the connections of Ba_{xs} , PHP and JO_2 at the
275 ANTARES/EMSO-LO observatory site in the northwestern Mediterranean Sea during the

276 BATMAN (2016) cruise. Our results reveal a strong relationship between Ba_{xs} contents and
277 measured JO_2 rates. Also, DWA Ba_{xs} vs. column integrated PHP, as well as measured vs. Ba_{xs} -
278 based JO_2 relationships follow trends previously reported in the Southern Ocean where the
279 Dehairs's function was first established to estimate POC remineralisation rate. Results from the
280 present study would indicate that this function can also be applied in the Mediterranean basin
281 provided that adequate Ba_{xs} background values are estimated. From a global climate perspective,
282 the Ba_{xs} tool will help to better balance the MedSea water column C budget. It will contribute to
283 gain focus on the emerging picture of the C transfer efficiency (strength of the biological pump).

284

285 **DATA AVAILABILITY**

286 All data and metadata will be made available at the French INSU/CNRS LEFE CYBER
287 database (scientific coordinator: Hervé Claustre; data manager, webmaster: Catherine
288 Schmechtig). INSU/CNRSLEFE CYBER (2020)

289

290 **AUTHOR CONTRIBUTION**

291 SJ and DL designed the experiment for JO_2 . SJ, CT and MG designed the experiments for PHP
292 measurements. SJ and FLM managed barium sampling during the cruise. NB managed CTD
293 deployment at sea. MG, SG and MR managed PHP. All co-authors contributed to writing.

294

295 **COMPETING INTERESTS**

296 The authors declare that they have no known competing financial interests or personal
297 relationships that could have appeared to influence the work reported in this paper.

298

299 **ACKNOWLEDGEMENTS**

300 We thank the officers and crew of *R/V EUROPE* for their assistance during work at sea. This
301 research was supported by the French national LEFE/INSU "REPAP" project (PI. S. Jacquet). It
302 was co-funded by the "ROBIN" project (PIs. C. Tamburini, F.A.C. Le Moigne) of Labex OT-

303 Med (ANR-11-LABEX-0061) funded by the Investissements d'Avenir and the French
304 Government project of the ANR, through the A*Midex project (ANR-11-IDEX-0001-02).
305 Authors have benefited of the support of the SNO-MOOSE and SAM-MIO. BATMAN is a
306 contribution to the "AT – POMPE BIOLOGIQUE" of the Mediterranean Institute of
307 Oceanography (MIO) and to the international IMBER program. The instrument (ELEMENT XR,
308 ThermoFisher) was supported in 2012 by European Regional Development Fund (ERDF).
309

310 **Figure captions**

311 Figure 1: (a) Schematic representation of the convergence of the different estimators of oxygen
312 consumption and C remineralization rates from the “oxygen dynamics”, “barium proxy” and
313 “prokaryotic activity” tools; (b) Location of the BATMAN cruise at the ANTARES observatory
314 site in the NW-Mediterranean Sea (42°48'N, 6°10'E). The location of the DYFAMED station is
315 reported for comparison (Sternberg et al., 2008); (c) Potential temperature - salinity - depth plots
316 and isopycals for BATMAN profiles. SW : Surface Water, WIW : Winter Intermediate Water,
317 LIW : Levantine Intermediate Water, DMW : Deep Mediterranean Water. Graph constructed
318 using Ocean Data View (Schlitzer, 2002; Ocean Data View; [http://www.awi-](http://www.awi-bremerhaven.de/GEO/ODV)
319 [bremerhaven.de/GEO/ODV](http://www.awi-bremerhaven.de/GEO/ODV))

320

321 Figure 2: (a) Particulate biogenic Ba_{xs} (pM) and particulate Al (nM) profiles next to the biogenic
322 Ba fraction (%) in the upper 1000 m at ANTARES. The grey area represents a biogenic Ba
323 fraction larger than 80 %. BKG: Ba_{xs} background. Ba_{xs} profile (pM) at DYFAMED : data from
324 Sternberg et al. (2008); (b) ANTARES ratio plot (green square) of integrated PHP in the upper
325 100 m over integrated PHP in the upper 500 m versus depth-weighted average (DWA)
326 mesopelagic Ba_{xs} (pM) over the 100-500m depth interval. Regression of the same ratio is
327 reported for KEOPS1 (light blue symbols; out plateau stations) and KEOPS2 (dark blue symbols;
328 Southern Ocean, Jacquet et al., 2015) and #DY032 (red square; PAP station, NE-Atlantic; pers.
329 data) cruises. The blue line represents the trend obtained during KEOPS2 (Jacquet et al., 2015).

330

331 Figure 3: (a) Relationship between Ba_{xs} concentrations (pM) and oxygen consumption rates
332 ($\mu\text{mol L}^{-1} \text{d}^{-1}$) from optodes measurements (JO_2 -Opt) at ANTARES; (b) Confrontation of oxygen
333 consumption rates (JO_2 ; $\text{mmol m}^{-2} \text{d}^{-1}$) obtained from different methods: optodes measurements

334 (this study; green square) and dark community respiration DCR (winkler titration; red triangles;
335 $\text{JO}_2\text{-DCR}$; Jacquet et al., 2015; KEOPS1), and Dehairs's transfer function calculation (Dehairs et
336 al., 1997) based on Ba_{xs} contents. The black line corresponds to the correlation obtained during
337 KEOPS1 (Jacquet et al., 2015); (c) Dehairs's relationship between depth-weighted average
338 (DWA) mesopelagic Ba_{xs} (pM) and JO_2 ($\mu\text{mol L}^{-1} \text{ d}^{-1}$) compared to ANTARES result (this
339 study), KEOPS1 data (Southern Ocean; Jacquet et al., 2015) and GEOVIDE correlation (North
340 Atlantic; Lemaitre et al., 2018).

341

342 **References**

343 Bertram, Miriam, and James P. Cowen. "Morphological and Compositional Evidence for Biotic
344 Precipitation of Marine Barite." *Journal of Marine Research* 55 (1997): 577–93.

345 Broecker, Wallace S. "'NO', a Conservative Water-Mass Tracer." *Earth and Planetary Science
346 Letters* 23, no. 1 (August 1974): 100–107. doi:10.1016/0012-821X(74)90036-3.

347 Buesseler, Ken O., and Philip W. Boyd. "Shedding Light on Processes That Control Particle
348 Export and Flux Attenuation in the Twilight Zone of the Open Ocean." *Limnology and
349 Oceanography* 54, no. 4 (2009): 1210–32. doi:10.4319/lo.2009.54.4.1210.

350 Cardinal, Damien, Frank Dehairs, Thierry Cattaldo, and Luc André. "Geochemistry of Suspended
351 Particles in the Subantarctic and Polar Frontal Zones South of Australia: Constraints on
352 Export and Advection Processes." *Journal of Geophysical Research: Oceans* 106, no. C12
353 (décembre 2001): 31637–56. doi:10.1029/2000JC000251.

354 **Cardinal D.**, Savoye N., Trull T. W., André L., Kopczynska E. E., and Dehairs F.: Variations of
355 carbon remineralisation in the Southern Ocean illustrated by the Baxs proxy, Deep-Sea Res.
356 Pt. I, 52, 355–370, <https://doi.org/10.1016/j.dsr.2004.10.002>, 2005.

357 Dehairs, F., R. Chesselet, and J. Jedwab. "Discrete Suspended Particles of Barite and the Barium
358 Cycle in the Open Ocean." *Earth and Planetary Science Letters* 49, no. 2 (September 1980):
359 528–50. doi:10.1016/0012-821X(80)90094-1.

360 Dehairs, F., S. Jacquet, N. Savoye, B. A. S. Van Mooy, K. O. Buesseler, J. K. B. Bishop, C. H.
361 Lamborg, et al. "Barium in Twilight Zone Suspended Matter as a Potential Proxy for

362 Particulate Organic Carbon Remineralization: Results for the North Pacific.” *Deep Sea*
363 *Research Part II: Topical Studies in Oceanography*, Understanding the Ocean’s Biological
364 Pump:results from VERTIGO, 55, no. 14–15 (juillet 2008): 1673–83.
365 doi:10.1016/j.dsr2.2008.04.020.

366 Dehairs, F., C. E. Lambert, R. Chesselet, and N. Risler. “The Biological Production of Marine
367 Suspended Barite and the Barium Cycle in the Western Mediterranean Sea.”
368 *Biogeochemistry* 4, no. 2 (June 1, 1987): 119–40. doi:10.1007/BF02180151.

369 Dehairs, F., D. Shopova, S. Ober, C. Veth, and L. Goeyens. “Particulate Barium Stocks and
370 Oxygen Consumption in the Southern Ocean Mesopelagic Water Column during Spring and
371 Early Summer: Relationship with Export Production.” *Deep Sea Research Part II: Topical*
372 *Studies in Oceanography* 44, no. 1–2 (1997): 497–516. doi:10.1016/S0967-0645(96)00072-
373 0.

374 Ellison, Eurachem/CITAC Guide CG4, Quantifying Uncertainty in Analytical Measurement.
375 Eds. S.L.R. Ellison, M. Rosslein and A. Williams. Second edition ISBN 0948926 15 5, Pp
376 120, 2000.

377 Giering, Sarah L. C., Richard Sanders, Richard S. Lampitt, Thomas R. Anderson, Christian Tamburini,
378 Mehdi Boutrif, Mikhail V. Zubkov, et al. “Reconciliation of the Carbon Budget in the Ocean’s
379 Twilight Zone.” *Nature* 507, no. 7493 (March 27, 2014): 480–83.

380 Hainbucher, D., A. Rubino, V. Cardin, T. Tanhua, K. Schroeder, and M. Bensi. “Hydrographic
381 Situation during Cruise M84/3 and P414 (spring 2011) in the Mediterranean Sea.” *Ocean*
382 *Sci.* 10, no. 4 (juillet 2014): 669–82. doi:10.5194/os-10-669-2014.

383 Henson, Stephanie A., Richard Sanders, Esben Madsen, Paul J. Morris, Frédéric Le Moigne, and
384 Graham D. Quartly. "A Reduced Estimate of the Strength of the Ocean's Biological Carbon
385 Pump." *Geophysical Research Letters* 38, no. 4 (février 2011): L04606.
386 doi:10.1029/2011GL046735.

387 IPCC Working Group 1, 5th Assessment Report (AR5) Climate Change 2013, Published in Jan.
388 2014.

389 **Jacquet** S.H.M., Dehairs F., Dumont I., Becquevort S., Cavagna A.-J., Cardinal, D.: Twilight
390 zone organic carbon remineralization in the Polar Front Zone and Subantarctic Zone south
391 of Tasmania, *Deep-Sea Res. Pt. II*, 58, 2222–2234, <https://doi.org/10.1016/j.dsr2.2011.05.029>,
392 2011.

393 Jacquet, S. H. M., F. Dehairs, D. Lefèvre, A. J. Cavagna, F. Planchon, U. Christaki, L. Monin, L.
394 André, I. Closset, and D. Cardinal. "Early Spring Mesopelagic Carbon Remineralization and
395 Transfer Efficiency in the Naturally Iron-Fertilized Kerguelen Area." *Biogeosciences* 12, no.
396 6 (March 17, 2015): 1713–31. doi:10.5194/bg-12-1713-2015.

397 Jacquet, S. H. M., F. Dehairs, N. Savoye, I. Obernosterer, U. Christaki, C. Monnin, and D.
398 Cardinal. "Mesopelagic Organic Carbon Remineralization in the Kerguelen Plateau Region
399 Tracked by Biogenic Particulate Ba." *Deep Sea Research Part II: Topical Studies in
400 Oceanography*, KEOPS: Kerguelen Ocean and Plateau compared Study, 55, no. 5–7 (March
401 2008): 868–79. doi:10.1016/j.dsr2.2007.12.038, 2008b

402 Jacquet, S. H. M., J. Henjes, F. Dehairs, A. Worobiec, N. Savoye, and D. Cardinal. "Particulate
403 Ba-Barite and Acantharians in the Southern Ocean during the European Iron Fertilization

404 Experiment (EIFEX).” *Journal of Geophysical Research* 112, no. G4 (October 23, 2007).
405 doi:10.1029/2006JG000394.

406 Jacquet, S.H.M., C. Monnin, V. Riou, L. Jullion, and T. Tanhua. “A High Resolution and Quasi-
407 Zonal Transect of Dissolved Ba in the Mediterranean Sea.” *Marine Chemistry* 178 (January
408 20, 2016): 1–7. doi:10.1016/j.marchem.2015.12.001.

409 **Jacquet** S.H.M., Savoye N., Dehairs F., Strass V.H., Cardinal D.: Mesopelagic carbon remineralization
410 during the European Iron Fertilization Experiment, *Global Biogeochem. Cy.*, 22, 1–9,
411 <https://doi.org/10.1029/2006GB002902>, **2008a**.

412 Jullion, L., S. H. M. Jacquet, and T. Tanhua. “Untangling Biogeochemical Processes from the
413 Impact of Ocean Circulation: First Insight on the Mediterranean Dissolved Barium
414 Dynamics.” *Global Biogeochemical Cycles* 31, no. 8 (2017): 1256–70.
415 doi:10.1002/2016GB005489.

416 Kirchman DL (1993) Leucine incorporation as a measure of biomass production by heterotrophic
417 bacteria. In: Kemp PF, Sherr BF, Sherr EB, Cole JJ (eds) *Handbooks of methods in aquatic*
418 *microbial ecology*. Lewis Publishers, Boca Raton, Ann Arbor, London, Tokyo, p 509–512

419 Lemaitre, N., H. Planquette, F. Planchon, G. Sarthou, S. Jacquet, M. I. García-Ibáñez, A.
420 Gourain, et al. “Particulate Barium Tracing of Significant Mesopelagic Carbon
421 Remineralisation in the North Atlantic.” *Biogeosciences* 15, no. 8 (2018): 2289–2307.
422 doi:10.5194/bg-15-2289-2018.

423 Malanotte-Rizzoli, P., V. Artale, G. L. Borzelli-Eusebi, S. Brenner, A. Crise, M. Gacic, N. Kress,
424 et al. “Physical Forcing and Physical/biochemical Variability of the Mediterranean Sea: A

425 Review of Unresolved Issues and Directions for Future Research.” *Ocean Science* 10, no. 3
426 (2014): 281–322. doi:10.5194/os-10-281-2014.

427 Martin, John H., George A. Knauer, David M. Karl, and William W. Broenkow. “VERTEX:
428 Carbon Cycling in the Northeast Pacific.” *Deep Sea Research Part A. Oceanographic
429 Research Papers* 34, no. 2 (1987): 267–85. doi:[http://dx.doi.org/10.1016/0198-0149\(87\)90086-0](http://dx.doi.org/10.1016/0198-0149(87)90086-0).

431 Martinez-Ruiz, Francisca, Fadwa Jroundi, Adina Paytan, Isabel Guerra-Tschuschke, María del
432 Mar Abad, and María Teresa González-Muñoz. “Barium Bioaccumulation by Bacterial
433 Biofilms and Implications for Ba Cycling and Use of Ba Proxies.” *Nature Communications*
434 9, no. 1 (April 24, 2018): 1619. doi:10.1038/s41467-018-04069-z.

435 Martinez-Ruiz, F., A. Paytan, M.T. Gonzalez-Muñoz, F. Jroundi, M.M. Abad, P.J. Lam, J.K.B.
436 Bishop, T.J. Horner, P.L. Morton, and M. Kastner. “Barite Formation in the Ocean: Origin
437 of Amorphous and Crystalline Precipitates.” *Chemical Geology* 511 (April 20, 2019): 441–
438 51. doi:10.1016/j.chemgeo.2018.09.011.

439 Ramondenc, Simon, Goutx Madeleine, Fabien Lombard, Chiara Santinelli, Lars Stemmann,
440 Gabriel Gorsky, and Lionel Guidi. “An Initial Carbon Export Assessment in the
441 Mediterranean Sea Based on Drifting Sediment Traps and the Underwater Vision Profiler
442 Data Sets.” *Deep Sea Research Part I: Oceanographic Research Papers* 117 (November
443 2016): 107–19. doi:10.1016/j.dsr.2016.08.015.

444 Sanchez-Vidal, A., R. W. Collier, A. Calafat, J. Fabres, and M. Canals (2005), Particulate barium
445 fluxes on the continental margin: A study from the Alboran Sea (Western Mediterranean),
446 Mar. Chem., 93, 105–117.

447 Santinelli, Chiara, Luciano Nannicini, and Alfredo Seritti. “DOC Dynamics in the Meso and Bathypelagic
448 Layers of the Mediterranean Sea.” *Deep Sea Research Part II: Topical Studies in Oceanography*,
449 Ecological and Biogeochemical Interactions in the Dark Ocean, 57, no. 16 (août 2010): 1446–59.
450 doi:10.1016/j.dsr2.2010.02.014.

451 Siegel DA, Buesseler KO, Behrenfeld MJ, Benitez-Nelson CR, Boss E, Brzezinski MA, Burd A, Carlson
452 CA, D'Asaro EA, Doney SC, Perry MJ, Stanley RHR and Steinberg DK (2016) Prediction of the
453 Export and Fate of Global Ocean Net Primary Production: The EXPORTS Science Plan. *Front. Mar.*
454 *Sci.* 3:22. doi: 10.3389/fmars.2016.00022

455 Simon M, Azam F (1989) Protein content and protein synthesis rates of planktonic marine
456 bacteria. *Mar Ecol Prog Ser* 51:201–213

457 Shopova, D., F. Dehairs, and W. Baeyens. “A Simple Model of Biogeochemical Element
458 Distribution in the Oceanic Water Column.” *Journal of Marine Systems* 6, no. 4 (juin 1995):
459 331–44. doi:10.1016/0924-7963(94)00032-7.

460 Speicher, E. A., S. B. Moran, A. B. Burd, R. Delfanti, H. Kaberi, R. P. Kelly, C. Papucci, et al.
461 “Particulate Organic Carbon Export Fluxes and Size-Fractionated POC/234Th Ratios in the
462 Ligurian, Tyrrhenian and Aegean Seas.” *Deep Sea Research Part I: Oceanographic*
463 *Research Papers* 53, no. 11 (2006): 1810–30.
464 doi:<http://dx.doi.org/10.1016/j.dsr.2006.08.005>.

465 Sternberg, E., C. Jeandel, E. Robin, and M. Souhaut. "Seasonal Cycle of Suspended Barite in the
466 Mediterranean Sea." *Geochimica et Cosmochimica Acta* 72, no. 16 (2008): 4020–34.
467 doi:<https://doi.org/10.1016/j.gca.2008.05.043>.

468 Tamburini C, Canals M, Durieu de Madron X, Houpert L, Lefèvre D, Martini S, D'Ortenzio F,
469 Robert A, Testor P, and the ANTARES collaboration (2013) Deep-sea bioluminescence
470 blooms after dense water formation at the ocean surface. PLoS One 8:e67523

471 Tamburini C, Garcin J, Ragot M, Bianchi A (2002) Biopolymer hydrolysis and bacterial
472 production under ambient hydrostatic pressure through a 2000 m water column in the NW
473 Mediterranean. Deep Res II 49:2109–2123

474 Taylor, S.R., McLennan, S.M.: The continental crust: its composition and evolution, Blackwell
475 Scientific Publications, 312pp, 1985.

476

477

478

479

480

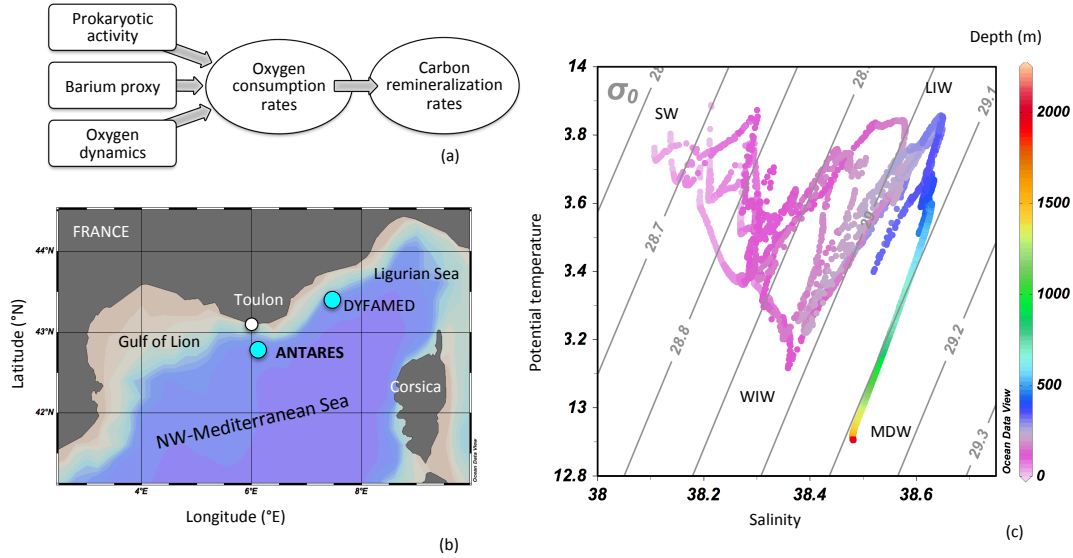
481

482

483

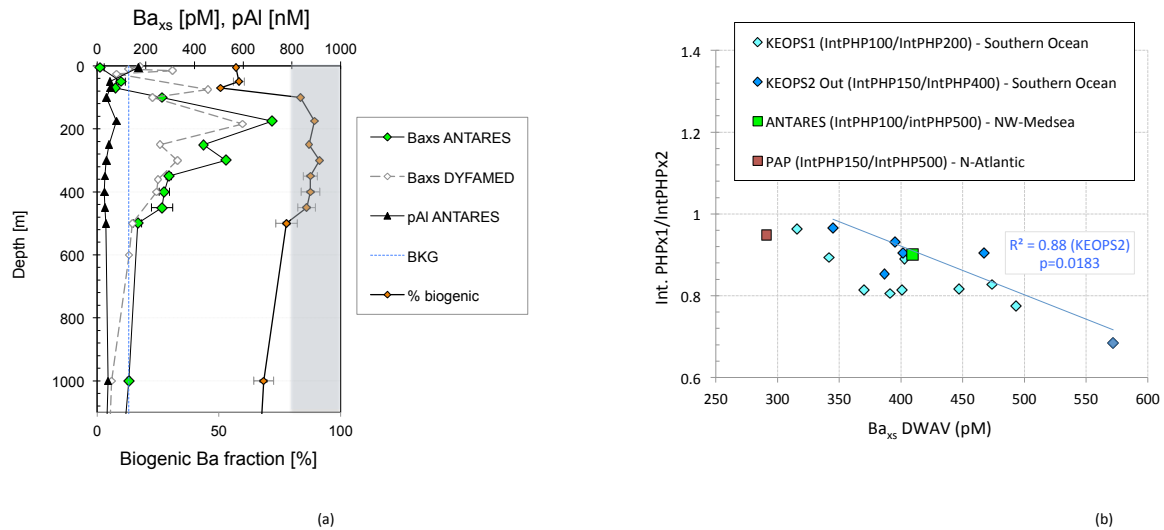
484

485 FIGURE 1



486

487 FIGURE 2



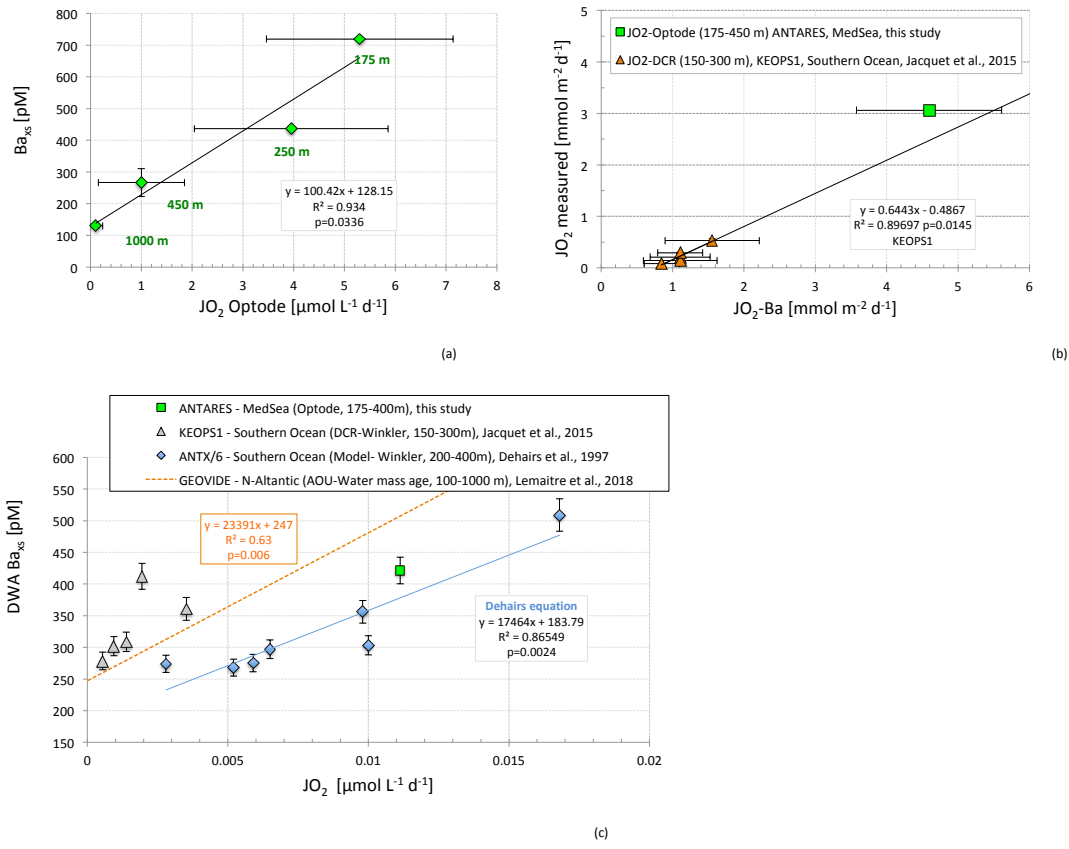
488

489

490

491 FIGURE 3

492



493

494

495